Segmenting Overlapping Red Blood Cells With Classical Image Processing and Deep Learning

Nils Brünggel, Pascal Vallotton[a] and Patrick Conway
Roche Diagnostics

Keywords: Machine Learning, Deep Learning, Semantic Segmentation, Hematology.

Abstract: In hematology the ability to count and analyze red blood cells (RBCs) is of major importance. Roche's proprietary Bloodhound® technology allows the automated printing and staining of slides to generate a monolayer of blood cells. While the RBCs are spread evenly, overlaps cannot be avoided completely. In the presence of such overlaps several tasks become problematic such as counting cells, quantifying the mean cellular volume or measuring cell shapes, critical for particular conditions such as anisocytosis (RBCs that are unequal in size) or rouleaux (clumps of RBCs that look like stacked coins). Modern deep learning models such as U-Net make it possible to accurately segment images given the appropriate training data (images and segmentation masks). The U-Net paper highlights the ability to train a model with only few images by applying data augmentation. We apply the learnings from their work and show that the mask creation can largely be automated: We collected images of free-standing RBCs, automatically segmented these using traditional image processing algorithms and combined these to generate artificial overlaps. We then used these images to train a model and show that it generalizes to real overlaps.

1 INTRODUCTION

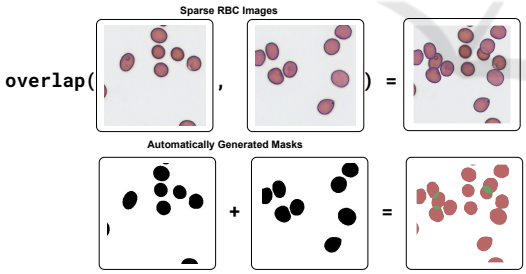

Figure 1: Images of non-overlapping RBCs can easily be segmented. Those images are then combined to generate artificial overlaps. The masks are summed to obtain a three-class mask.

To analyze a blood sample for hematological disorders, a medical technologist traditionally creates a blood smear on a glass slide. The smear is made with an automated slide maker or by manually dispearsing a drop of blood on a slide. In the so called feathered edge region of the blood smear, the cells should be spread evenly; allowing the microscopic analysis of these cells. This region is also referred to as a monolayer (see (Bain, 2014), chapter 1 for details). Most red blood cells (RBCs) in the monolayer are free-standing. However it is common to find overlapping RBCs and clumps as well. The cells at the beginning and end of the smear are squashed together and cannot be examined. We exclude these cells in our analysis and focus on the cells in the monolayer.

Roche's proprietary Bloodhound® technology allows the automated printing and staining of blood, creating a monolayer of cells (Bruegel et al., 2018). The cells are spread evenly across the whole print, only the cells at the border are squashed together. RBC overlaps cannot be avoided completely either: In the presence of such overlaps several tasks become problematic such as counting cells, quantifying the mean cellular volume or measuring cell shapes relevant for particular conditions such as anisocytosis (RBCs that are unequal in size) or rouleaux (clumped RBCs that resemble a stack of coins, see (Bain, 2014) chapter 3, page 97 for more information). Since we print whole blood, sometimes platelets and white blood cells (WBCs) can be seen too. In this work we focus on segmenting RBCs, therefore WBCs and platelets belong to the background class.

Modern deep learning models such as U-Net (Ronneberger et al., 2015) showed that it is possi-

[a] https://orcid.org/0000-0002-4159-1447

ble to accurately segment biomedical images given the appropriate training data (images and pixel-wise segmentation masks). The U-Net paper highlights the ability to train a model with only few images by applying data augmentation. We apply these learnings and focus on the automatic creation of masks: We collected images of free-standing RBCs, automatically segmented these using traditional image processing and combined these to create artificial overlaps. We then use these artificial images to train a U-Net model and show that it generalizes to real overlaps.

2 RELATED WORK

The introduction of deep learning methodology specifically to the analysis of overlapping RBCs is relatively recent, so the literature on the topic is still sparse. Most publications on this topic use classical image processing algorithms (for example (Naruenatthanaset et al., 2021) or (Moallem et al., 2018)). Recently, Zhang et al. (2020) used a modified U-Net to segment and classify RBCs with various abnormal shapes. They observed that a vanilla U-Net often makes three types of errors when segmenting RBC images into background and cell classes:

1. Failure to properly separate non-touching cells.
2. Artefacts (such as dirt spots) segmented as cells.
3. Incompletely segmented cells.

It should be noted that these errors often do not affect common performance metrics (eg IOU) by much, because the vast majority of pixels are still classified correctly with these errors present. They describe the use of deformable convolutions (originally introduced by Dai et al. (2017)) which can learn to adapt their receptive fields. Using their "deformable U-Net" they are able to lower the rate of these errors by large margins. Combining their approach with our ground truth generation technique is a potential research direction.

Another recent deep learning approach exploited a combination of U-Net foreground mask with Faster R-CNN (Kassim et al., 2021). This allowed the authors to reach impressive red blood cell counting performance on malaria smear images. To the best of our knowledge, our approach to ground truth mask generation has not been described in a deep learning context yet.

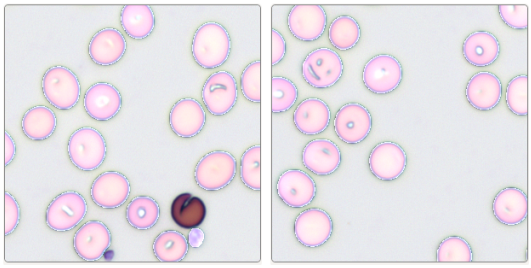

Figure 2: Shows the mask review app. Most of the automatically generated masks are correct (right), but there are a few mistakes (left): An RBC is missing and a platelet is wrongly classified as RBC.

3 MATERIALS AND METHODS

3.1 Data Collection

We collected 2'300 image crops (300x300 pixels) of non-overlapping red blood cells from a Romanowsky stained slide. The full frame images (2024x1512 pixels) were manually selected to ensure that they contain no overlaps. From those we randomly cropped out squares images for model training. The slides were printed and stained using Roche's proprietary slide printing method (Bruegel et al., 2018). For imaging we used an automated microscope with a 20x magnification. The images were then segmented by a simple algorithm that involves edge detection with a Laplacian filter (OpenCV Team, 2020), the removal of small objects and a binary opening. After the initial segmentation we reviewed the images and corrected the few masks that had mistakes in it. For this we developed a webapp that shows the image with the mask overlay to the user (see figure 2). For mask correction we used the freely available GNU Image Manipulation Program (GIMP) (Kimball and Mattis, 2018) and overlaid the binary mask as a separate layer on top of the image.

3.2 Artificial Overlaps

By overlapping every (non-overlapping) RBC image with every other RBC image, we could create a very large dataset from just a few real images. However we noticed that if we only do that, the model quickly overfits to the training and validation set and does not generalize to real overlaps. Instead it is important to understand the visual variations of RBC overlaps that can typically be found on microscopic images. Figure 4 shows two different kinds of overlaps: The two cells marked in red simply overlap: The cell on the top partially occludes the cell below. The two cells marked in blue look like they are fused together.

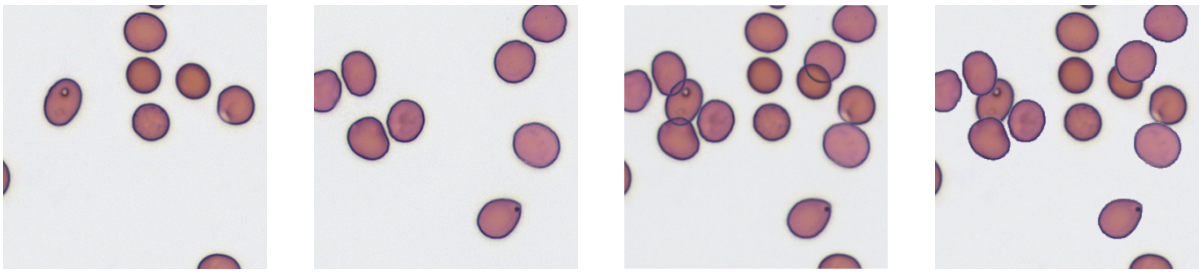

(a) first image (b) second image (c) min(a, b) (d) b over a

Figure 3: Simulated overlaps: Using two images with non-overlapping RBCs (a and b) we can generate two types of overlaps (image c and d).

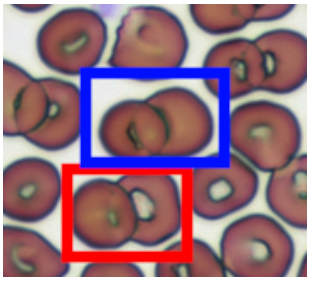

Figure 4: Real RBCs overlaps, note that the overlaps marked in red and blue are visually very different.

We found that these two types of overlaps can largely be simulated by either taking the minimum of both images (figure 3, c) or by drawing the RBCs from one image over the other image (figure 3, d). Note that when comparing these images to figure 4 they look somewhat synthetic: In image c the edges of both cells are very sharp and clearly visible in the overlapping region, this is not the case in the real example where the edge of the right cell on the left side of the overlap is not always clearly visible (marked in blue). In image d the edges of the cell on the top are very sharp in the overlapping area. In the actual overlap they appear a bit softer (figure 4, marked in red). The sharp edge in image d is caused by cutting out the RBC using a binary mask which leads to an immediate large change in color values.

We also simulate Rouleaux by overlapping images with themselves, moved by a few pixels (randomly chosen between 20 and 30) in a randomly chosen direction.

Empirically, we found that two additional steps are needed to create images that can be used to train a model that generalizes to images with real overlaps:

1. Combine both types of overlaps with a weighted sum, where the weight is drawn from a bathtub shaped distribution: We noticed that the real overlaps never exactly look like the artificial overlaps in figure 3 (image c and d; compare this to the real overlaps in figure 4). But the cases where either the cell at the bottom is almost invisible in the region of the overlap or that both cells are clearly visible dominate. More precisely we use the following formula to calculate the final image:

$$a \sim Beta(\alpha, \beta)$$
$$i = a \cdot i_{min} + (1-a) \cdot i_{over},$$

where i is the final image and i_{min} and i_{over} are the artificial overlaps as explained above. We chose α and β to be 0.7 to obtain a bathtub shaped beta distribution.

2. Randomly choose 50% of the generated images for blurring. Apply Gaussian blur to the chosen images with $\sigma \in [1,2]$ (uniformly chosen).

3.3 Dataset

The final dataset we used for training consists of the following parts:

1. Artificial overlaps: For each image of the 2'300 collected images we randomly chose another image and overlap it according to the procedure described above.
2. Artificial rouleaux: 30 images (again randomly chosen) that are overlapped with itself to simulate rouleaux.
3. Manually corrected masks: 12 images from another slide that contain many overlapping RBCs. The masks were obtained by running an earlier model and then fixing all the mistakes in these masks manually.

3.4 Data Augmentation and Traning

We used fastai's (Howard and Gugger, 2020) U-Net implementation which takes a modern backbone (e.g. ResNet 50) and turns it into a U-Net (Fastai Team, 2020b). Please note that this model differs in

the details from the original U-Net implementation: For example it does not include a dropout layer and it relies on PixelShuffle ICNR upsampling (Aitken et al., 2017) for artefact-free upsampling. The model was trained with fastai's data augmentation turned on (Howard and Gugger, 2020, chapter 5.5). We only differed from the default settings (Fastai Team, 2020a) by setting rotation to 5 degrees and enabling flips (horizontal and vertical). We used the vanilla cross-entropy loss function (PyTorch Team, 2020) from PyTorch (Paszke et al., 2019) for training.

4 RESULTS

We found an average pixel-wise intersection over union (IOU) on our validation set (20% random split from the training data) of 98.90%. Since the validation set consists mostly of artificial overlaps, this metric is not too informative. Instead it is interesting to look at cases of real overlaps. We created a test set consisting of RBC images with real overlaps from separate slides (with blood from other patients), none of which were included in the training or validation set. The images differ slightly from slide-to-slide because of print, stain and patient variations. The masks used to calculate the IOU were created as described in section 3.1 with the addition of manual annotated overlaps.

Table 1: IOUs for the normal RBC images, shown in figure 5 (bg stands for background and over for overlaps).

image	bg	rbc	over	mean
a	0.98	0.95	0.82	0.92
b	0.97	0.97	0.78	0.91
c	0.92	0.93	0.53	0.80

Figure 5 shows the predicted masks on a normal slide. The IOUs for each image are shown in table 1. The model predicts most of the RBCs (red) and overlaps (green) correctly. However there are a few mistakes: Part of a platelet was mistaken for an RBC (b) and not every RBC that sticks to the white blood cell at the top left could be segmented correctly (c). We found some cases where the initial segmentation algorithm confused platelets with RBCs (see figure 2), which could be the reason for the wrongly segmented platelet in figure 5 b. The training set does not contain enough examples of overlapping RBCs that stick to white blood cells. This is probably the reason why the segmentation works poorly in this area.

Figure 6 shows the segmentation results on a slide with rouleaux. The IOUs for each image are shown in table 2. Note that most overlaps are predicted correctly. However the IOUs for the overlaps are lower, which is not surprising given that this is an abnormal case. There are a few cases where only part of the overlap was detected, hinting that the model can be improved with more data.

Table 2: IOUs for the rouleaux RBC images, shown in figure 6.

image	bg	rbc	over	mean
a	0.96	0.88	0.56	0.80
b	0.95	0.91	0.59	0.82
c	0.98	0.95	0.5	0.81

Table 3: IOUs for the test set consisting of 36 crops from 3 normal slides.

-	bg	rbc	over	mean
mean	0.96	0.96	0.65	0.86
std	0.02	0.02	0.11	0.04
min	0.90	0.89	0.21	0.72
max	0.99	0.98	0.79	0.91

For a quantitative evaluation we used three additional normal slides: From each slide we chose three full frame images that show a reasonable degree of RBC overlaps. We then randomly selected four crops from each image resulting in 12 crops per slide, 36 in total. The masks were created as described earlier. Table 3 shows the IOUs for each class across all image crops. The IOUs for background (bg) and RBCs are very high which is not surprising, given that we can segment freestanding RBCs easily with simple image processing. There are multiple reasons for the lower IOU for the overlap (over) class:

- Images with very few overlaps: If the model misses a small overlap in such an image the IOU will be very low. From the standard deviation (std), min and max rows it can be seen that the overlap IOU varies a lot between different images.
- Manual masks: It is very hard to correctly segment the overlaps down to individual pixels. By looking at a magnified image it is often not clear where exactly the overlap starts and ends.
- As described above the model still fails to correctly segment some overlaps, mitigating this aspect will require more data.

Summarizing the results in just a single metric only gives a very high level picture of how well the model actually performs. We encourage the interested reader to examine the provided dataset and code to investigate in detail how the model performs in each case we provide.

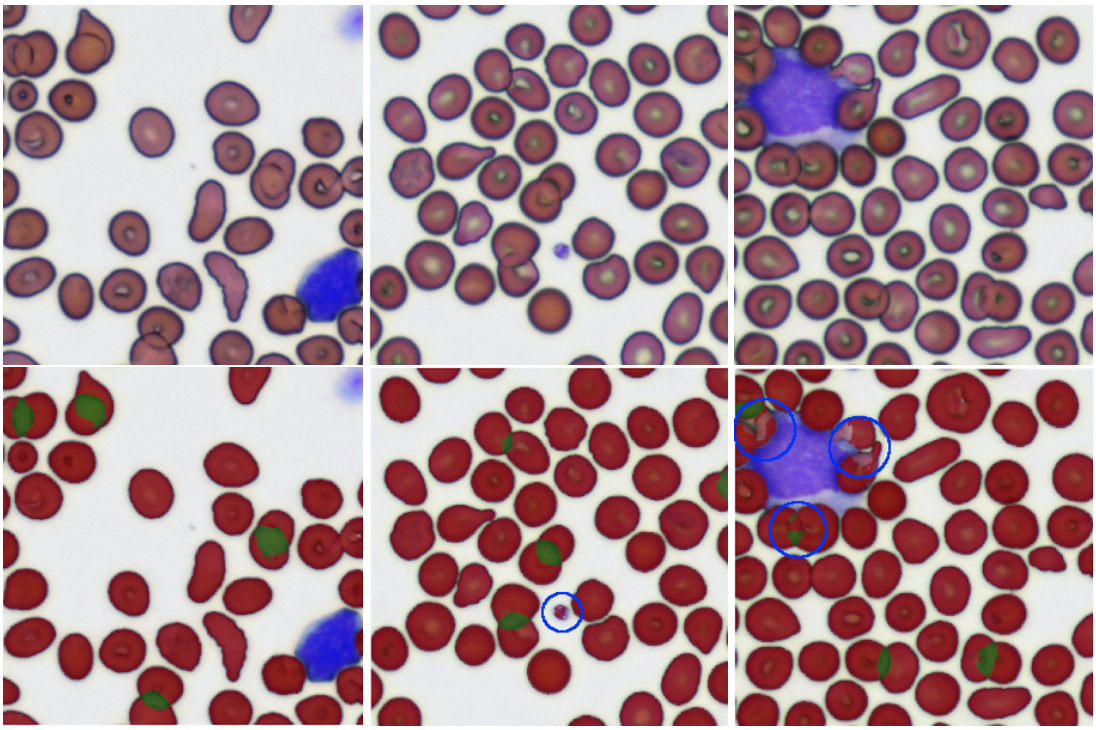

(a) (b) (c)

Figure 5: Segmentation results for a normal slide. The original image is shown above, below the same image is shown with the predicted mask overlaid. Segmentation mistakes are highlighted in blue.

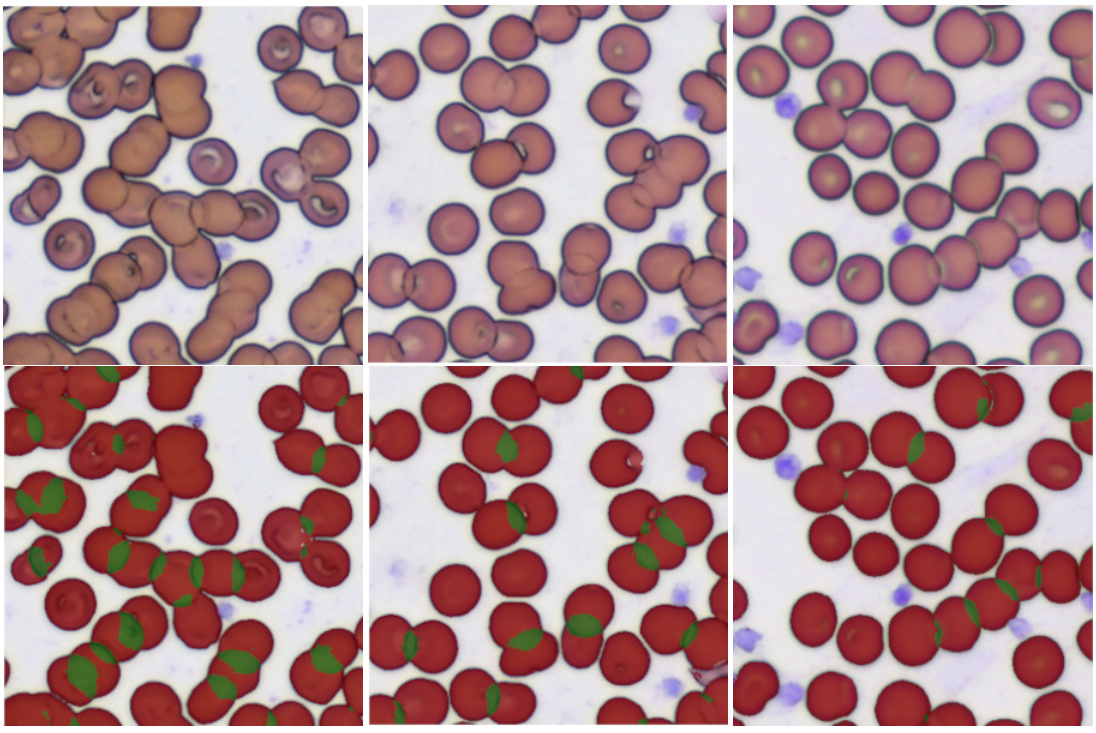

(a) (b) (c)

Figure 6: Segmentation results for a slide with rouleaux.

5 CONCLUSION

In this paper we show that the learning process can be bootstrapped with the automatic creation of masks. The path to improve the results is straightforward: The initial masks need to be reviewed and improved further (see section 2.1). More data needs to be added where the model fails. For example to teach the model to correctly segment RBCs that stick to white blood cells, more such images and segmentation masks are needed. The masks can be created by letting the already existing model predict most of the mask, making manual adjustments only necessary where the model fails to segment the cells correctly. To further improve model training one could also adopt more recent approaches to data augmentation such as RandAugment (Cubuk et al., 2019).

In the age of deep learning it is often forgotten that image processing tasks, such as biomedical image segmentation, can be solved to a large degree with a simple algorithm that does not require a parameterized model and a large training set. In our case we could solve the biggest part of the problem (segmenting free-standing RBCs) with just a few lines of code and use the resulting masks to generate enough training data to train a modern segmentation model.

ACKNOWLEDGEMENTS

We thank Anton Hasenkampf for carefully reviewing our draft.

REFERENCES

Aitken, A., Ledig, C., Theis, L., Caballero, J., Wang, Z., and Shi, W. (2017). Checkerboard artifact free sub-pixel convolution. page 16.

Bain, J., B. (2014). *Blood Cells: A Practical Guide*. 5 edition.

Bruegel, M., George, T. I., Feng, B., Allen, T. R., Bracco, D., Zahniser, D. J., and Russcher, H. (2018). Multicenter evaluation of the cobas m 511 integrated hematology analyzer. *Int J Lab Hem*, 40(6):672–682.

Cubuk, E. D., Zoph, B., Shlens, J., and Le, Q. V. (2019). RandAugment: Practical automated data augmentation with a reduced search space. *arXiv:1909.13719 [cs]*. arXiv: 1909.13719.

Dai, J., Qi, H., Xiong, Y., Li, Y., Zhang, G., Hu, H., and Wei, Y. (2017). Deformable Convolutional Networks. Number: arXiv:1703.06211 arXiv:1703.06211 [cs].

Fastai Team (2020a). `aug_transforms`. https://docs.fast.ai/vision.augment.html#aug_transforms. Last checked on June 6, 2022.

Fastai Team (2020b). `unet_learner`. https://docs.fast.ai/vision.learner.html#unet_learner. Last checked on June 6, 2022.

Howard, J. and Gugger, S. (2020). fastai: A Layered API for Deep Learning. *Information*, 11(2):108. arXiv: 2002.04688.

Kassim, Y. M., Palaniappan, K., Yang, F., Poostchi, M., Palaniappan, N., Maude, R. J., Antani, S., and Jaeger, S. (2021). Clustering-Based Dual Deep Learning Architecture for Detecting Red Blood Cells in Malaria Diagnostic Smears. *IEEE J. Biomed. Health Inform.*, 25(5):1735–1746.

Kimball, S. and Mattis, P. (2018). Gimp (GNU Image Manipulation Program).

Moallem, G., Sari-Sarraf, H., Poostchi, M., Maude, R. J., Silamut, K., Antani, S., Thoma, G., Jaeger, S., and Amir Hossain, M. (2018). Detecting and segmenting overlapping red blood cells in microscopic images of thin blood smears. In Gurcan, M. N. and Tomaszewski, J. E., editors, *Medical Imaging 2018: Digital Pathology*, page 50, Houston, United States. SPIE.

Naruenatthanaset, K., Chalidabhongse, T. H., Palasuwan, D., Anantrasirichai, N., and Palasuwan, A. (2021). Red Blood Cell Segmentation with Overlapping Cell Separation and Classification on Imbalanced Dataset. *arXiv:2012.01321 [cs, eess]*.

OpenCV Team (2020). `cv::Laplacian`. https://docs.opencv.org/4.6.0/d4/d86/group__imgproc__filter.html#gad78703e4c8fe703d479c1860d76429e6. Last checked on June 14, 2022.

Paszke, A., Gross, S., Massa, F., Lerer, A., Bradbury, J., Chanan, G., Killeen, T., Lin, Z., Gimelshein, N., Antiga, L., Desmaison, A., Köpf, A., Yang, E., DeVito, Z., Raison, M., Tejani, A., Chilamkurthy, S., Steiner, B., Fang, L., Bai, J., and Chintala, S. (2019). PyTorch: An Imperative Style, High-Performance Deep Learning Library. *arXiv:1912.01703 [cs, stat]*. arXiv: 1912.01703.

PyTorch Team (2020). `torch.nn.CrossEntropyLoss`. https://pytorch.org/docs/stable/generated/torch.nn.CrossEntropyLoss.html. Last checked on June 6, 2022.

Ronneberger, O., Fischer, P., and Brox, T. (2015). U-Net: Convolutional Networks for Biomedical Image Segmentation. *arXiv:1505.04597 [cs]*.

Zhang, M., Li, X., Xu, M., and Li, Q. (2020). Automated Semantic Segmentation of Red Blood Cells for Sickle Cell Disease. *IEEE J. Biomed. Health Inform.*, 24(11):3095–3102.